Floris, I.; Calderón García, PA.; Sales Maicas, S.; Adam, JM. (2019). Effects of core position uncertainty on optical shape sensor accuracy. Measurement. 139:21-33. https://doi.org/10.1016/j.measurement.2019.03.031

Effects of core position uncertainty on Optical Shape Sensor accuracy

Ignazio Floris [a,b], Pedro A. Calderón [b], Salvador Sales [a], Jose M. Adam [b]*

[a]ITEAM , Universitat Politècnica de València, Camino de Vera s/n, Valencia, 46022, Spain
[b]ICITECH, Universitat Politècnica de València, Camino de Vera s/n, Valencia, 46022, Spain

Abstract

Optical fiber sensors are now widely recognized as extremely reliable instruments to sense strain. Optical shape sensors consist of multiple single-core optical fibers or multicore optical fibers capable of sensing bending direction and curvature by comparing the longitudinal strain of different cores in an instrumented section and reconstructing the sensor shape.
This paper describes a study on the effects of core position errors on the precision of optical shape sensors when measuring strain, bending direction and curvature, and identifies the role of measured curvature and core spacing (distance between section center and external cores), considering 7, 4, and 3-core fiber geometries, three of those most widely employed for sensing applications. The Monte Carlo technique was utilized to reproduce the measurement process. Forty-five simulations, including $3 \cdot 10^6$ trials, were carried out for each geometry with the aim of investigating the law of uncertainty propagation.
The results of the analysis, applicable to both multiple single-core fibers and multicore optical sensors equipped with distributed or quasi-distributed strain-sensors, show the effects of core position uncertainty and will be useful for new sensor designs and user options by predicting the achievable performance of these devices.

Keywords: Data Processing; Optical Fiber Sensor; Distributed sensing; Multicore Optical Fiber; Bending Sensor; Fiber optic shape sensing; Monte Carlo Method.

1. Introduction

Thanks to recent development, Optical Fiber Sensors (OFS) have been successfully employed in civil and industrial engineering [1–4] as well as in many chemical and medical [5,6] applications. Such a development is driven by the inherent advantages of OFS over conventional electrical sensors, which include immunity to electromagnetic interference (EMI), compactness and light weight, intrinsic safety, and resistance to harsh temperatures, radiation and chemicals.

Optical shape sensors consist of multiple single-core optical fibers or multicore optical fibers (an optional central core and some external cores displaced from the sensor axis) that can calculate the sensor shape. Even though both bending and torsion of the sensor can be determined by using only three non-aligned cores [7–9], additional cores can be employed to achieve better accuracy. The sensor shape can thus be calculated through the numerical integration of Frenet-Serret formulas [10]. High accuracy in sensing bending direction and curvature is crucial to calculate the torsion $\tau(s)$ and curvature $\kappa(s)$ functions and obtain a reliable estimation of the 3D shape of the sensor.

* Corresponding author.
E-mail address: joadmar@upv.es (J.M. Adam)

A number of fiber optic sensors have been developed to sense curvature and shape, including: a highly sensitive fiber optic inclinometer to sense 3D deformation based on three distributed optical fiber sensors fixed to the tube wall [11]. Wang et al. designed an inclinometer to monitor landslides, based on four optical fibers with fiber Bragg gratings (FBG) inscribed and fixed to an aluminum tube [12]. Multicore Fiber (MCF) sensors, consisting of various cores inside a single cladding, are capable of high-accuracy curvature and shape sensing and have been applied in civil, mechanical, medical, and aerospace engineering. Villatoro et al. monitored the verticality of towers, bridge piles, and buildings by using an ultrasensitive curvature sensor based on MCF [13]. A bending MCF sensor for displacement detection has been employed for tunnel health monitoring [14]. Fender et al. developed a two-axis temperature-insensitive accelerometer based on a multicore fiber curvature sensor [15]. MCF shape sensors can lead to improvements in biomedical techniques that need real-time shape and position calculation of surgical instruments with extremely high accuracy, as for instance catheters [16]. Lally et al. employed MCF sensors for flexible structures monitoring, including suspension bridges and aircraft wings [17].

Although electrical strain gauges can also be used to sense curvature and 3D shape [18–20], OFS are more compact, electrically safe and immune to electro-magnetic interferences.

In previous work the authors studied the effects of strain measurement uncertainty on sensing bending direction and curvature by means of one of the most widely employed multicore fiber geometries with different core spacing for sensing applications [21]. At the present time they are continuing their research on shape sensing within the H2020-MSCA-ITN FINESSE framework [22], focusing on the influence of core position uncertainty, another crucial aspect of shape sensor accuracy, and extending the investigation to multiple single-core optical fiber sensors and different section geometries, once again highlighting the role of core spacing and the measured curvature in the phenomenon.

Core position errors are due to errors in the manufacturing process. In MCF, they are in the range between a few hundred nanometers to one micrometer [23,24] and depend on the optical fiber drawing technique and the production equipment. The errors are higher and are related to the fastening technique in fiber bundles and shape sensors made with multiple single-core optical fibers, as the fibers are first manufactured and then fastened.

This paper proposes an algorithm using the Monte Carlo method to simulate the real position of the cores, supposing that they are affected by random errors with a Gaussian distribution, characterized by different standard deviations (SD) [25,26]. The strain values measured in the cores, if measurement uncertainty only depends on errors in core positions, were determined through calculating the strain function, considering different distances between the sensor axis and the outer cores (core spacing), different sensed curvature and distinct sensor section geometries: 3, 4 and 7-core. The distribution of longitudinal strain, curvature and bending direction angle (angle between the bending direction and the axis x) were also determined with a view to determining the contribution of core position errors to shape sensor inaccuracy.

The propagation laws of core position uncertainty in calculating the longitudinal strain, curvature and bending direction were successfully identified, although this information is frequently absent from the manufacturers' datasheets. The influence of core spacing, measured curvature and number of cores on these factors was also determined.

The research findings can be applied to both multiple single-core optical fibers sensors and multicore optical fiber sensors equipped with distributed or quasi-distributed strain-sensors, or to shape-sensing arrays in general. The relationships between measurement precision and the standard deviation of core position errors, core spacing and measured curvature are given at the end of the paper and are expected to be of assistance to manufacturers in designing new shape sensors and MCFs and to users when evaluating shape sensor performance.

2. Strain function calculation

Fiber optic sensors with several cores capable of strain sensing can be utilized for shape calculation. The natural frame of the curve coincides with the material sensor frame, when the sensor is fastened only at one extremity and the constraints are frictionless [27]. To reconstruct the sensor shape, the deformation of several sections along the sensor length must then be determined from the strain detected in the cores. To do this, it is supposed that the errors made by approximating with a constant value the strain along the length where it is sensed (the length of the FBG for quasi-distributed sensors or the spatial resolution for distributed strain sensors) are negligible.

In most cases, it is possible to assume that along the entire section the temperature is constant, considered the small core spacing, so that no temperature compensation is necessary (the correctness of this hypothesis should be ascertained for optical shape sensors with large radius). Therefore, if the sensor is bent and external twisting is prevented (no local twisting forces are induced in the sensor), strain varies linearly along the whole section, under the Kirchhoff rod assumption. The strain function, $\varepsilon(x,y)$ (see Eq. 1), which describes how strain varies along the section (strain surface) is thus a plane, as shown in Fig 1, and can be determined if the strain of at least three non-aligned cores is known.

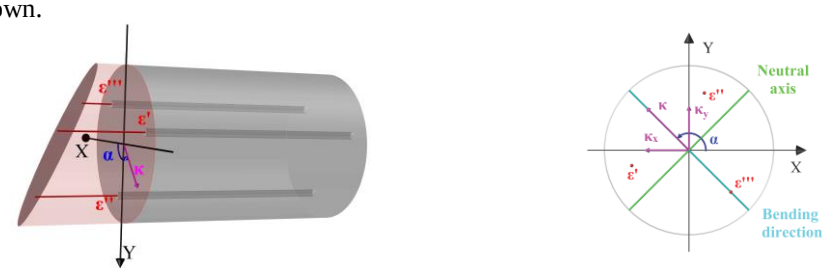

(a) (b)

Fig. 1.(a) 3D Strain distribution for a generic sensor where the strain is sensed at 3 points, by way of example; (b) Cross section.

The equation of the strain distribution, $\varepsilon(x,y)$, in a generic section, is defined when the longitudinal strain of the section is known (average strain, $avg(\varepsilon)$),ε^{long}, and the two components of curvature, κ_x and κ_y, with respect to the reference axes of the section, x and y, or the magnitude of the vector curvature, $|\kappa|$, and the bending direction angle, α, which identifies the bending direction:

$$\varepsilon(x,y) = a + bx + cy \qquad where\ \ a = \varepsilon^{long}; b = \kappa_x; c = \kappa_y; \tag{1}$$

where a, b, and c are the coefficients of the equation of the strain plane, equal to, respectively, the longitudinal strain, ε^{long}, and the two components of curvature, κ_x and κ_y, since they are the partial derivatives of $\varepsilon(x,y)$ with respect to x and y:

$$\kappa_x = \partial\varepsilon(x,y)/\partial x \ ; \ \kappa_y = \partial\varepsilon(x,y)/\partial y \tag{2}$$

If the strain is sensed at only 3 points (three-core sensor), the equation of the strain plane can be calculated by replacing the coordinates of the cores and the values of strain measured and obtaining a system of three linear equation.

When n cores are available, the strain is detected at n points and the strain function can be calculated by minimizing the Sum of Squared Errors (SSE), as shown in the following Equations:

$$SSE(a,b,c) = \sum_{i=1}^{n}(\varepsilon_i - a - bx_i - cy_i)^2 \tag{3}$$

$$\nabla SSE(a,b,c) = 0 \tag{4}$$

$$\begin{cases} \frac{\partial SSE(a,b,c)}{\partial a} = 0 \rightarrow na + b\sum_{i=1}^{n} x_i + c\sum_{i=1}^{n} y_i = \sum_{i=1}^{n} \varepsilon_i \\ \frac{\partial SSE(a,b,c)}{\partial b} = 0 \rightarrow a\sum_{i=1}^{n} x_i + b\sum_{i=1}^{n} x_i^2 + c\sum_{i=1}^{n} x_i y_i = \sum_{i=1}^{n} x_i \varepsilon_i \\ \frac{\partial SSE(a,b,c)}{\partial c} = 0 \rightarrow a\sum_{i=1}^{n} y_i + b\sum_{i=1}^{n} x_i y_i + c\sum_{i=1}^{n} y_i^2 = \sum_{i=1}^{n} y_i \varepsilon_i \end{cases} \tag{5}$$

The approach explained above is valid for all the section geometries with a generic number of cores *n* and without any symmetry, provided that there are at least three non-aligned cores. However, for the section geometries considered in this study, the system of equations becomes diagonal:

$$\begin{cases} na + 0 + 0 = \sum_{i=1}^{n} \varepsilon_i \\ 0 + b\sum_{i=1}^{n} x_i^2 + 0 = \sum_{i=1}^{n} x_i \varepsilon_i \\ 0 + 0 + c\sum_{i=1}^{n} y_i^2 = \sum_{i=1}^{n} y_i \varepsilon_i \end{cases} \tag{6}$$

Once the strain function equation has been determined, the magnitude of the vector curvature, $|\kappa|$, and the bending direction angle, α, can be calculated:

$$|\kappa| = \sqrt{\kappa_x^2 + \kappa_y^2} \tag{7}$$

$$\alpha = \tan^{-1}(\kappa_x/\kappa_y) \tag{8}$$

It should be pointed out that **a central core does not have any effect on the calculation of curvature and bending direction angle** (second and third equations of system), as its coordinates *x* and *y* are null, although it can be used to sense twisting [28].

3. Case study

3.1. Monte Carlo analysis and simulation

Widely accepted as an efficient problem solving tool, the Monte Carlo Method (MCM) is an experimental probabilistic technique designed to solve complex linear and nonlinear statistical or scientific problems [29–32]. As present-day computers can model considerable numbers of iterations with random results, the MCM, a broad set of computational and randomized algorithms, was created to deal with unpredictable processes and obtain numerical outcomes and the respective probability, based on repeated random sampling.

Despite the exactness of analytical methods, they are only suitable for simple cases, whereas identifying distribution propagation in complex problems requires approximations and simulations [26]. The Monte Carlo technique can be employed to compute the probability distribution of output data based on the assigned probability distributions of the input quantities on which the resulting variables are dependent, with the aim of determining the law of propagation [25,26]. For this purpose, before running the simulation, the input probability distribution has to be specified to generate the random sampling.

When applied to the propagation of uncertainty, the MCM mimics the real probabilistic measurement process by mean of the uncertainty of random sampling and generation hundreds of thousands of measures and resulting outcomes to individuate the relationship between the variables involved.

The MCM has previously been used to simulate optical curvature sensing [21,33]; it has been utilized, for instance, to mimic curvature gauges by means of ray tracing and identify the relationship between fiber curvature and light-loss.

In the present study, the MCM was employed to mimic the core position error, assuming that the errors that affect different cores and different sections are independent and uncorrelated, have only one random component and follow a standard normal distribution (the Gaussian probability distribution is the simulation input) with a certain standard deviation (SD). For each trial and in all the cores, the errors simulated were added to the correct value.

In multiple single-core optical fiber shape sensors, the core position errors are acquired during manufacture and depend on the optical fiber drawing technique, the production equipment used for the multicore fibers and fiber bundles, and on the technique used to fasten the fibers to the support (generally a tube), as well as the support's characteristics. Regrettably, manufacturers rarely provide information on any such errors.

3.2. Stopping rules

MCM effectiveness is a function of the number of trials in the simulation (sample size). When the number of samples increases, the simulation converges to a constant outcome and thus should be halted. Regrettably, the number of trials necessary for steady outcome cannot be theoretically calculated [34]. Nonetheless, in most cases a sample size between 10^5 and 10^6 replicates seem to be satisfactory [31,35]. Furthermore, a number of observations of 10^6 can commonly be envisaged to achieve a 95 % coverage probability for the output variable, so that this size is right to one or even two significant digits [26].

All the simulations in this research were performed with $3 \cdot 10^6$ replicates, considering a dataset composed of 3 subdatasets with 10^6 iterations each. To verify the statistical significance of the simulations, a comparison was drawn between the results of the total dataset and the ones obtained with the three subdatasets.

3.3. Sensor section geometry

The sensor section geometry, particularly the position and the number of the cores, has a considerable impact on the precision of the measured longitudinal strain, bending direction and curvature.

The multicore fibers available nowadays and suitable for shape sensing applications are lamentably limited, as, generally, they are the same produced for telecommunication applications. Their diameter is very small (regularly about 125 μm) and the core spacing is normally between 30 and 50 μm [8,10,13–17]. Manufacturing different MCF geometries for sensing purposes would be prohibitively expensive, considering that the sensors market is limited compared to the telecommunications one.

Since better accuracy can be achieved by increasing the core spacing, although less compact, optical shape sensors consisting of multiple optical fibers fastened to a support have been developed [11,12].

This study considered three of the most widely employed fiber geometries in sensing applications (see Fig. 2): a three- [10,11,13], four- [8,12,14,15,36] and seven-core section [16,23,28,37–39], with constant angular spacing and equal distance between the outer cores and the sensor axis, including 5 distinct core spacings: 30, 50, 70, 140 and 300μm.

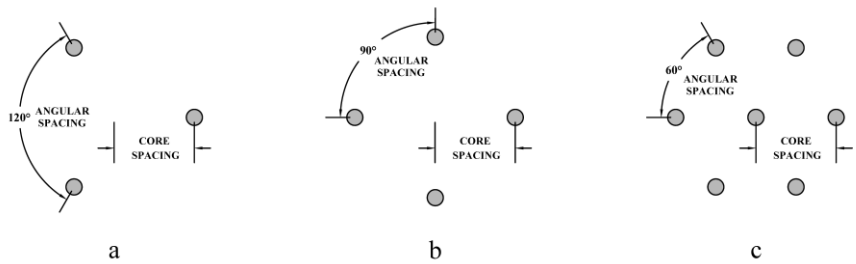

Fig. 2. (a) Three-core section geometry; (b) Four-core section geometry; (c) Seven-core section geometry.

3.4. Core position simulation errors

The core position error distribution in fiber optic sensors was modeled by the Monte Carlo method with 15 simulations and $3 \cdot 10^6$ iterations for each geometry. Three different standard deviations (SD) were considered to characterize the 3D standard normal distributions (the Gaussian probability distributions were the simulation inputs) of the errors and five distinct core spacings (distance between the sensor axis and the external cores).

By way of example, the 3D Gaussian frequency distribution of the core position for a seven-core geometry is shown in Fig. 3.

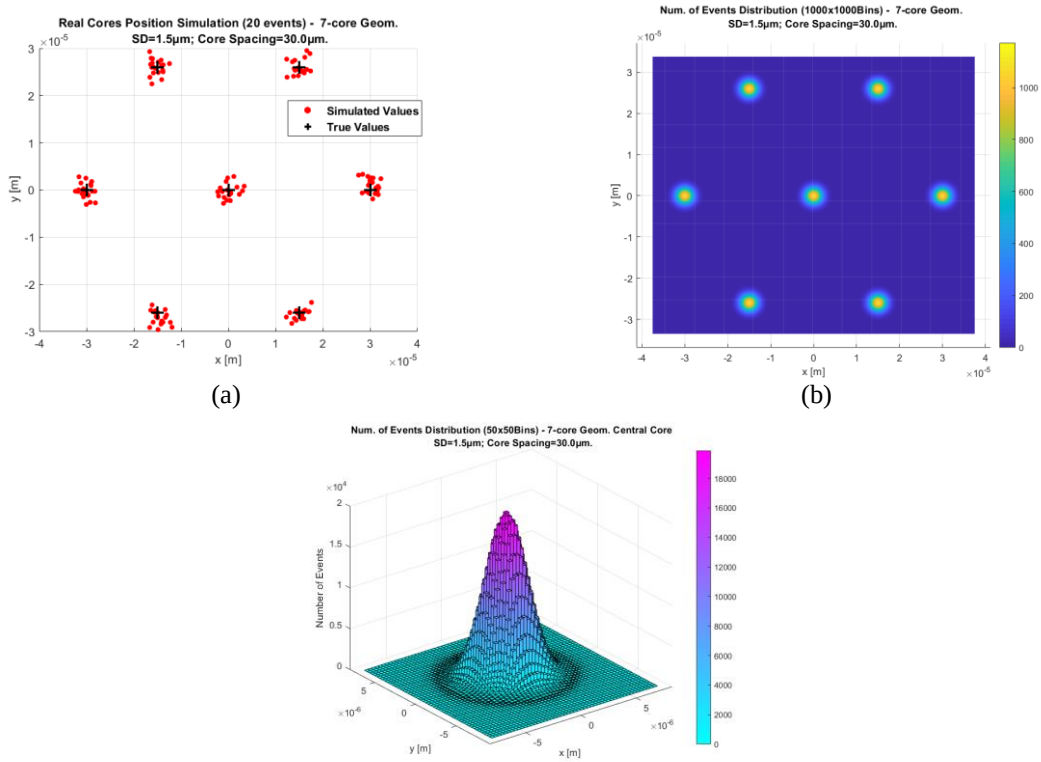

(a) (b) (c)

Fig. 3. (a) Real core position simulation of 7-core shape sensor (20 events; SD core position = 1.5 μm; Core spacing = 30 μm); Core position 3D frequency distribution ($3 \cdot 10^6$ events; SD core position = 1.5 μm; Core spacing = 30 μm) of a 7-core shape sensor, considering (b) all the seven cores; (c) only the central core.

3.5. Strain calculation

After generating the 3D frequency distribution of core positions, the input of the simulation, the distribution of the strain sensed by each core can be calculated, considering a certain state of deformation of the section and assuming that the uncertainty in strain sensing only depends on core position imprecision. The state of deformation can be defined by means of longitudinal strain, bending direction angle and curvature, ε^{long}, α and $|\kappa|$.

The strain sensed by a certain core in each iteration is the sum of two components: the longitudinal strain (average strain of the section) and the bending strain (see Eq. 9). The bending strain can be calculated as the shortest distance from the core to the neutral axis multiplied by the magnitude of the strain function gradient (curvature magnitude). The distance from the neutral axis is the abscissa of the point in a Cartesian coordinate system obtained by rotating the x and y axes counter clockwise through an angle α (see Fig. 1.b).

$$\varepsilon_i^j = \varepsilon^{long} + |\kappa| \left[x_i^j \cos\alpha + y_i^j \sin\alpha \right] \tag{9}$$

where i represents the core considered and j the iteration.

Fig. 4 shows the frequency distributions of the strain generated due to core position errors with an SD of 0.8 μm in the cores of a four-core sensor with core spacing of 30 μm when the measured curvature is 40 m^{-1} (2.5 cm radius of curvature).

It should be noted that the strain distributions are still Gaussian and that the SD may be much higher than the strain resolution of commercial OFS, which can reach a few microstrains, in the case considered it is 32 με.

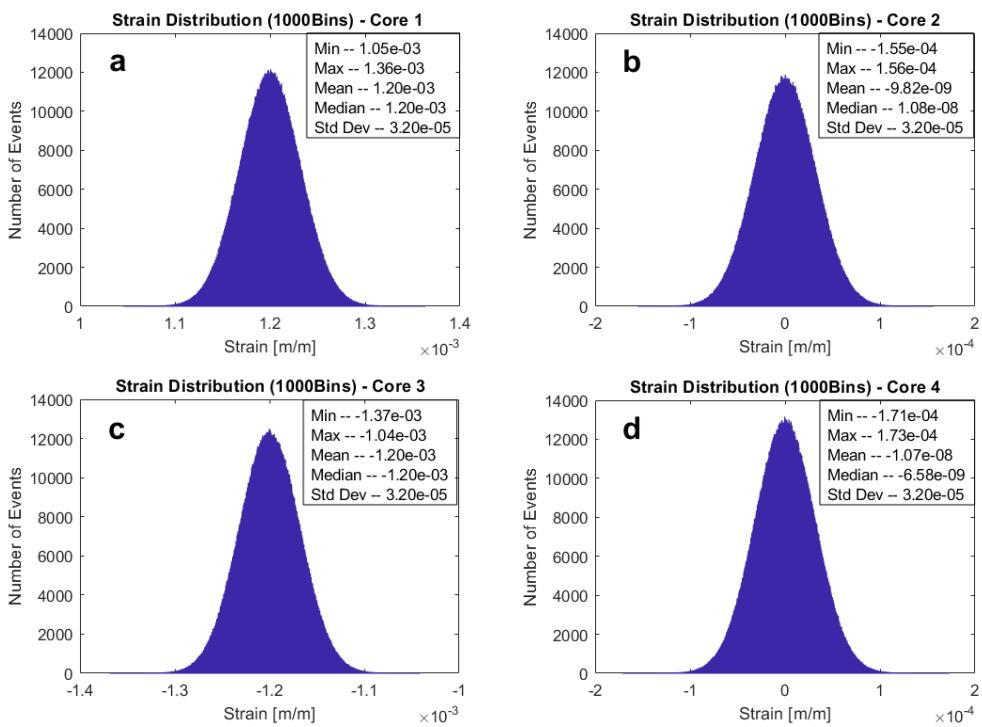

Fig. 4. Strain frequency distribution ($3 \cdot 10^6$ events; SD core position = 0.8μm; Core spacing = 30 μm; Measured curvature = 40.0 m^{-1}) of a 4-core shape sensor simulated in (a) Core 1; (b) Core 2; (c) Core 3; (d) Core 4.

4. Multi-step approach for calculating longitudinal strain, curvature and bending direction

An algorithm was designed in MATLAB® [40] to model the core position error distributions by the Monte Carlo technique and generate the consequent distribution of longitudinal strain, bending direction angle and curvature, taking into account three distinct fiber geometries. The procedure is summarized in the following steps:

- Step 1. Simulation of Gaussian frequency distribution of core position errors (Section 3.3) for each section geometry, considering five different core spacings and three different SD;
- Step 2. Calculation of strain distribution, by Eq. 9, based on the distributions of core position (x_i^j and y_i^j on every iteration), obtained in the previous step, and considering diverse section deformation states, definable through measured longitudinal strain, curvature and bending direction angle (coefficients of the strain plane equation), ε^{long}, $|\kappa|$ and α, as described in Section 2;
- Step 3. Determination of longitudinal strain, bending direction angle and curvature distributions by means of the equations given in Section 2, and tests of statistical significance;
- Step 4. Development of the predictive models.

To clarify the process, a specific example is provided considering the inputs of the first simulation for a three-core sensor (section geometry = 3-core; core spacing = 30.00 μm; SD core position = 0.20 μm; longitudinal strain = 0.00 με; curvature = 0.10 m^{-1}; bending direction angle = 0.00 rad).

First, the core position errors are simulated, according to the SD chosen (in this case 0.20 μm). The real core coordinates are calculated as sum of the exact coordinates, determined considering the geometrical features of the section, and the simulated errors, as shown in Table 1:

Table 1. Example of real core coordinates calculation.

	Exact Core Coordinates		**Example of Simulated Errors**		**Example of Real Core Coordinates**	
	x_i [μm]	**y_i [μm]**	**x_i [μm]**	**y_i [μm]**	**x_i [μm]**	**y_i [μm]**
Core 1	30.00	25.98	-0.009	0.303	29.99	26.28
Core 2	-15.00	-25.98	-0.145	0.276	-15.14	-25.70
Core 3	-15.00	0.00	-0.107	-0.279	-15.11	-0.28

Secondly, the strain detected in each core, taking into account the state of deformation of the section (in this example ε^{long} = 0.00 με, $|\kappa|$ = 0.10 m^{-1}, and α = 0.00 rad), is calculated by using Eq. 9. By way of illustration, the strain detected in core 1 is computed below:

$$\varepsilon_1 = \varepsilon^{long} + |\kappa|\,(x_1 cos\,\alpha + y_1 sin\,\alpha) = 0.00 + 0.10\,[29.99(cos\,0.00) + 26.28(sin\,0.00)] \quad (10)$$

To conclude, the strain detected in the cores, calculated as indicated above, and the simulated core coordinates arising from core position errors, are substituted into Eqs. 6. Thus, the longitudinal strain, ε^{long}, the magnitude of the vector curvature, $|\kappa|$, and the bending direction angle, α, now affected by the errors in core position, are determined by solving the system and using Eqs. 7-8.

In each simulation, this procedure was repeated for each of the $3 \cdot 10^6$ iterations, divided into three group (defined as subdataset) of 10^6 iteration each. Then, the SDs of the resulting distribution of

longitudinal strain, bending direction angle and curvature were determined considering the 3 subdatasets as well as the entire dataset, which consists of the three subdatasets (in other word all the data of the simulation), and a comparison was drawn to prove the statistical significance of the simulation, as explained in Section 5.3.

5. Results and comments

The outcomes of the experiments are presented this Section.

5.1. Outcome frequency distribution

45 simulations with $3 \cdot 10^6$ trials were carried out for each fiber geometry.
The inputs of the simulations were

1) Geometrical features of the section, as described in Section 3.2:
    a. Section geometry;
    b. Core spacing;
    c. Core position error normal frequency distribution with a certain SD.
2) State of deformation of the section (coefficients of the strain plane equation), which are the shape sensor's output measures:
    a. Longitudinal strain;
    b. Curvature;
    c. Bending direction angle.

The outcomes of the simulations are:

1) Frequency distribution of longitudinal strain;
2) Frequency distribution of curvature;
3) Frequency distribution of bending direction angle.

Fig. 5 shows an example of the distributions generated in a three-core sensor with core spacing of 30 µm due to core position errors with an SD of 0.8 µm, when the longitudinal strain, the bending direction angle and the curvature (inputs of the simulation) are respectively, 0.0 µm, 0.0 rad and 40 m^{-1}.

The resulting frequency distributions are clearly Gaussian and the mean values of the distributions coincide with the input of the simulation, showing that the model is well constructed and the number of iterations in the simulation is sufficient.

The propagation law of core position errors can thus be defined by considering only the SD of the distributions obtained in the simulation.

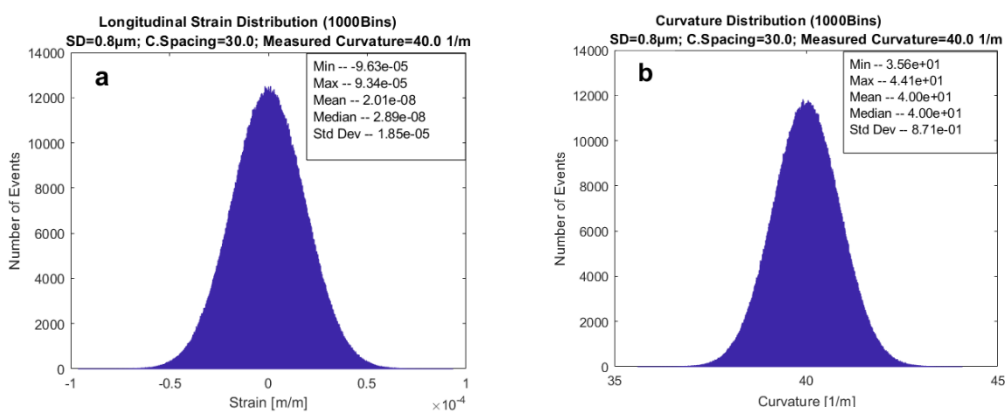

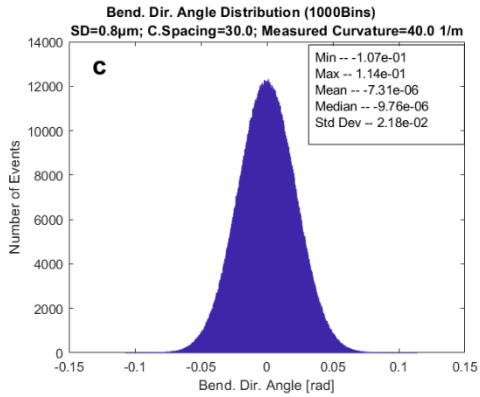

Fig. 5. Frequency distribution of (a) longitudinal strain, (b) curvature and (c) bending direction angle of a 3-core shape sensor ($3 \cdot 10^6$ events; SD core position = 0.8 μm; Core spacing = 30 μm; Measured curvature = 40.0 m^{-1}).

5.2. Simulation results

As the error distribution depends on the slope of the strain plane, the measured longitudinal strain has no influence on the simulation results. In fact, when there is no bending and the strain plane is parallel to the *xy* plane, the SD of the resulting distribution is null and the bending direction angle is not defined. In the same way, bending direction angle does not influence the resulting distributions, since it depends on the arbitrarily defined Cartesian coordinate system, being the angle between the *x* axis and the bending direction. These two parameters were thus set equal to zero in the simulations.

During the simulations it was found that the SD of the core position error distributions and the measured curvature have a linear influence on the phenomenon, whereas core spacing affects it nonlinearly. Three different measured curvatures and standard deviations (SD) of core position distribution along with five values of core spacings were thus considered in the study, as reported in Table 2.

The results of the simulations for three-core, four-core and seven-core geometries are listed in Tables 3-5.

Table 2. Inputs of the simulations.

Section Geometrical Features			**Strain Plane Coefficients**		
Section Geometry	**Core Spacing [μm]**	**SD Core Position Distr. [μm]**	**Measured Longitudinal Strain [με]**	**Measured Bend. Dir. Angle [rad]**	**Measured Curvature [1/m]**
	30.00				
Three-core	50.00	0.20			0.10
Four-core	70.00	0.80	0.00	0.00	5.00
Seven-core	140.00	1.50			40.00
	300.00				

321 **Table 3.** Results of the simulations for a three-core sensor.

Simulation N°	Core Spacing [µm]	SD Core Position [µm]	Measured Curvature [1/m]	SD Longitudinal Strain [µε]	SD Curvature [1/m]	SD Bend. Direction Angle [rad]
1	30.00	0.20	0.10	0.0116	0.0005	0.0054
2	30.00	0.20	5.00	0.5771	0.0272	0.0054
3	30.00	0.20	40.00	4.6204	0.2177	0.0054
4	30.00	0.80	0.10	0.0462	0.0022	0.0218
5	30.00	0.80	5.00	2.3066	0.1087	0.0218
6	30.00	0.80	40.00	18.4694	0.8714	0.0218
7	30.00	1.50	0.10	0.0866	0.0041	0.0408
8	30.00	1.50	5.00	4.3284	0.2041	0.0409
9	30.00	1.50	40.00	34.6075	1.6336	0.0409
10	50.00	0.20	0.10	0.0115	0.0003	0.0033
11	50.00	0.20	5.00	0.5775	0.0163	0.0033
12	50.00	0.20	40.00	4.6220	0.1307	0.0033
13	50.00	0.80	0.10	0.0462	0.0013	0.0131
14	50.00	0.80	5.00	2.3099	0.0654	0.0131
15	50.00	0.80	40.00	18.4932	0.5224	0.0131
16	50.00	1.50	0.10	0.0865	0.0025	0.0245
17	50.00	1.50	5.00	4.3298	0.1225	0.0245
18	50.00	1.50	40.00	34.6471	0.9793	0.0245
19	70.00	0.20	0.10	0.0116	0.0002	0.0023
20	70.00	0.20	5.00	0.5778	0.0117	0.0023
21	70.00	0.20	40.00	4.6148	0.0933	0.0023
22	70.00	0.80	0.10	0.0462	0.0009	0.0093
23	70.00	0.80	5.00	2.3095	0.0466	0.0093
24	70.00	0.80	40.00	18.4857	0.3732	0.0093
25	70.00	1.50	0.10	0.0866	0.0017	0.0175
26	70.00	1.50	5.00	4.3327	0.0874	0.0175
27	70.00	1.50	40.00	34.6400	0.6996	0.0175
28	140.00	0.20	0.10	0.0115	0.0001	0.0012
29	140.00	0.20	5.00	0.5776	0.0058	0.0012
30	140.00	0.20	40.00	4.6225	0.0467	0.0012
31	140.00	0.80	0.10	0.0462	0.0005	0.0047
32	140.00	0.80	5.00	2.3093	0.0233	0.0047
33	140.00	0.80	40.00	18.4788	0.1867	0.0047
34	140.00	1.50	0.10	0.0866	0.0009	0.0087
35	140.00	1.50	5.00	4.3293	0.0437	0.0088
36	140.00	1.50	40.00	34.6410	0.3498	0.0087
37	300.00	0.20	0.10	0.0116	0.0001	0.0005
38	300.00	0.20	5.00	0.5770	0.0027	0.0005
39	300.00	0.20	40.00	4.6163	0.0218	0.0005
40	300.00	0.80	0.10	0.0462	0.0002	0.0022
41	300.00	0.80	5.00	2.3092	0.0109	0.0022
42	300.00	0.80	40.00	18.4676	0.0871	0.0022
43	300.00	1.50	0.10	0.0867	0.0004	0.0041
44	300.00	1.50	5.00	4.3310	0.0204	0.0041
45	300.00	1.50	40.00	34.6495	0.1633	0.0041

322

323

324

325 **Table 4.** Results of the simulations for a four-core sensor.

Simulation N°	Core Spacing [µm]	SD Core Position [µm]	Measured Curvature [1/m]	SD Longitudinal Strain [µε]	SD Curvature [1/m]	SD Bend. Direction Angle [rad]
1	30.00	0.20	0.10	0.0100	0.0005	0.0047
2	30.00	0.20	5.00	0.5001	0.0236	0.0047
3	30.00	0.20	40.00	3.9991	0.1887	0.0047
4	30.00	0.80	0.10	0.0400	0.0019	0.0189
5	30.00	0.80	5.00	1.9989	0.0943	0.0189
6	30.00	0.80	40.00	16.0044	0.7541	0.0189
7	30.00	1.50	0.10	0.0750	0.0035	0.0354
8	30.00	1.50	5.00	3.7510	0.1768	0.0354
9	30.00	1.50	40.00	30.0010	1.4135	0.0354
10	50.00	0.20	0.10	0.0100	0.0003	0.0028
11	50.00	0.20	5.00	0.5004	0.0141	0.0028
12	50.00	0.20	40.00	4.0021	0.1132	0.0028
13	50.00	0.80	0.10	0.0400	0.0011	0.0113
14	50.00	0.80	5.00	1.9989	0.0566	0.0113
15	50.00	0.80	40.00	15.9892	0.4526	0.0113
16	50.00	1.50	0.10	0.0750	0.0021	0.0212
17	50.00	1.50	5.00	3.7508	0.1060	0.0212
18	50.00	1.50	40.00	30.0103	0.8483	0.0212
19	70.00	0.20	0.10	0.0100	0.0002	0.0020
20	70.00	0.20	5.00	0.5004	0.0101	0.0020
21	70.00	0.20	40.00	3.9994	0.0807	0.0020
22	70.00	0.80	0.10	0.0400	0.0008	0.0081
23	70.00	0.80	5.00	2.0007	0.0404	0.0081
24	70.00	0.80	40.00	15.9967	0.3235	0.0081
25	70.00	1.50	0.10	0.0750	0.0015	0.0151
26	70.00	1.50	5.00	3.7499	0.0757	0.0151
27	70.00	1.50	40.00	30.0081	0.6065	0.0152
28	140.00	0.20	0.10	0.0100	0.0001	0.0010
29	140.00	0.20	5.00	0.5001	0.0050	0.0010
30	140.00	0.20	40.00	3.9993	0.0404	0.0010
31	140.00	0.80	0.10	0.0400	0.0004	0.0040
32	140.00	0.80	5.00	1.9990	0.0202	0.0040
33	140.00	0.80	40.00	15.9995	0.1615	0.0040
34	140.00	1.50	0.10	0.0750	0.0008	0.0076
35	140.00	1.50	5.00	3.7529	0.0379	0.0076
36	140.00	1.50	40.00	29.9950	0.3031	0.0076
37	300.00	0.20	0.10	0.0100	0.0000	0.0005
38	300.00	0.20	5.00	0.5001	0.0024	0.0005
39	300.00	0.20	40.00	4.0008	0.0189	0.0005
40	300.00	0.80	0.10	0.0400	0.0002	0.0019
41	300.00	0.80	5.00	1.9991	0.0094	0.0019
42	300.00	0.80	40.00	15.9932	0.0754	0.0019
43	300.00	1.50	0.10	0.0750	0.0004	0.0035
44	300.00	1.50	5.00	3.7487	0.0177	0.0035
45	300.00	1.50	40.00	30.0062	0.1414	0.0035

326

327

328 **Table 5.** Results of the simulations for a seven-core sensor.

Simulation N°	Core Spacing [µm]	SD Core Position [µm]	Measured Curvature [1/m]	SD Longitudinal Strain [µε]	SD Curvature [1/m]	SD Bend. Direction Angle [rad]
1	30.00	0.20	0.10	0.0076	0.0004	0.0039
2	30.00	0.20	5.00	0.3780	0.0192	0.0038
3	30.00	0.20	40.00	3.0238	0.1540	0.0038
4	30.00	0.80	0.10	0.0302	0.0015	0.0154
5	30.00	0.80	5.00	1.5117	0.0770	0.0154
6	30.00	0.80	40.00	12.0815	0.6158	0.0154
7	30.00	1.50	0.10	0.0567	0.0029	0.0289
8	30.00	1.50	5.00	2.8363	0.1442	0.0289
9	30.00	1.50	40.00	22.6819	1.1552	0.0289
10	50.00	0.20	0.10	0.0076	0.0002	0.0023
11	50.00	0.20	5.00	0.3781	0.0115	0.0023
12	50.00	0.20	40.00	3.0246	0.0924	0.0023
13	50.00	0.80	0.10	0.0302	0.0009	0.0092
14	50.00	0.80	5.00	1.5122	0.0462	0.0092
15	50.00	0.80	40.00	12.0875	0.3695	0.0092
16	50.00	1.50	0.10	0.0567	0.0017	0.0173
17	50.00	1.50	5.00	2.8336	0.0865	0.0173
18	50.00	1.50	40.00	22.6794	0.6927	0.0173
19	70.00	0.20	0.10	0.0076	0.0002	0.0017
20	70.00	0.20	5.00	0.3781	0.0082	0.0016
21	70.00	0.20	40.00	3.0214	0.0660	0.0016
22	70.00	0.80	0.10	0.0302	0.0007	0.0066
23	70.00	0.80	5.00	1.5118	0.0330	0.0066
24	70.00	0.80	40.00	12.1000	0.2642	0.0066
25	70.00	1.50	0.10	0.0567	0.0012	0.0124
26	70.00	1.50	5.00	2.8335	0.0619	0.0124
27	70.00	1.50	40.00	22.6942	0.4947	0.0124
28	140.00	0.20	0.10	0.0076	0.0001	0.0008
29	140.00	0.20	5.00	0.3781	0.0041	0.0008
30	140.00	0.20	40.00	3.0242	0.0330	0.0008
31	140.00	0.80	0.10	0.0302	0.0003	0.0033
32	140.00	0.80	5.00	1.5118	0.0165	0.0033
33	140.00	0.80	40.00	12.0985	0.1319	0.0033
34	140.00	1.50	0.10	0.0567	0.0006	0.0062
35	140.00	1.50	5.00	2.8355	0.0309	0.0062
36	140.00	1.50	40.00	22.6826	0.2476	0.0062
37	300.00	0.20	0.10	0.0076	0.0000	0.0004
38	300.00	0.20	5.00	0.3781	0.0019	0.0004
39	300.00	0.20	40.00	3.0244	0.0154	0.0004
40	300.00	0.80	0.10	0.0303	0.0002	0.0015
41	300.00	0.80	5.00	1.5105	0.0077	0.0015
42	300.00	0.80	40.00	12.0911	0.0616	0.0015
43	300.00	1.50	0.10	0.0567	0.0003	0.0029
44	300.00	1.50	5.00	2.8353	0.0144	0.0029
45	300.00	1.50	40.00	22.6951	0.1154	0.0029

329

330 *5.3. Statistical significance test*

331 As previously explained (Section 3.2), MCM needs a stopping rule to define the number of
332 iterations of the simulations (sample size). As the appropriate sample size necessary for steady
333 outcome cannot be theoretically calculated [34], beforehand, it was opted for $3 \cdot 10^6$, which in most
334 cases seem to be satisfactory [31]. To verify the correctness of the assumption, for each simulation,

a comparison was drawn between the standard deviations of the distributions obtained from the total dataset and the 3 subdatasets with 10^6 trials each.

The percentage error between the SDs of the subdatasets and the total dataset was determined by Eq. 10:

$$E = [(SD^T - SD^S)/SD^T]100 \tag{11}$$

where E is the percentage error and the standard deviation of the total dataset and the subdataset are respectively SD^T and SD^S. The highest value of percentage error considering all the simulations of this study is, in absolute terms, 0.198, proving the statistical significance of the simulations.

5.4. Curve Fitting Models

The relation between the SD of the frequency distribution of longitudinal strain, bending direction angle and curvature (dependent variables) and SD of the frequency distribution of core position errors, measured curvature and core spacing (independent variables) were identified with two variable curves using the Curve Fitting MATLAB® [40] Toolbox™. A sequence of three models (one for each dependent variable) were calibrated for each section geometry, fitting the results of the simulations, to identify the propagation law of core position uncertainty, determine the mathematical relationship between the considered variables and make the research outcomes more fruitful and user-friendly. The coefficient equations were estimated by a nonlinear regression analysis, based on the errors, including the Coefficient of Determination (R^2), Root-Mean-Square Error (RMSE) and Sum of Squared Errors (SSE):

$$R^2 = 1 - \frac{\sum_i (t_i - o_i)^2}{\sum_i (o_i)^2} \tag{12}$$

$$RMSE = \sqrt{\frac{1}{n}\sum_i (t_i - O_i)^2} \tag{13}$$

$$SSE = \sum_i (t_i - O_i)^2 \tag{14}$$

where t_i is the target value, O_i is the predicted value, and n is the number of data.

The first parameters identified were those that influence the standard deviation of the frequency distribution of longitudinal strain, bending direction and curvature. The curvature frequency distribution was found to be influenced by all three parameters, while core spacing did not influence the longitudinal strain distribution SD, nor did bending direction angle frequency distribution depend on the measured curvature.

The model equations were thus defined *a priori* and their performance, based on the errors, investigated *a posteriori*. In all cases, it was found that one coefficient was sufficient to efficiently fit the data.

The function that represents the dependence between longitudinal strain distribution SD and core position SD and measured curvature (see Eq. 15) was fitted with the coefficient k_1. Fig. 6 shows the surface fitting for the three-core section, by way of example.

Likewise, the function that defines the bending direction angle SD in terms of core position SD and core spacing (see. Eq. 17) was determined using the coefficient k_3, as shown in Fig. 7.

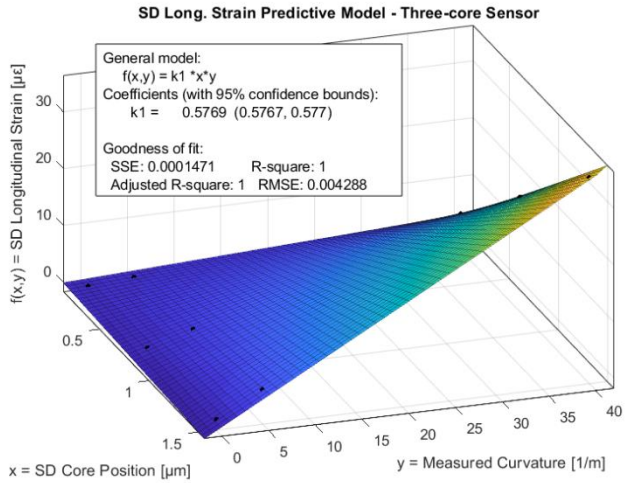

Fig. 6. Longitudinal strain SD curve-fitting for a three-core sensor.

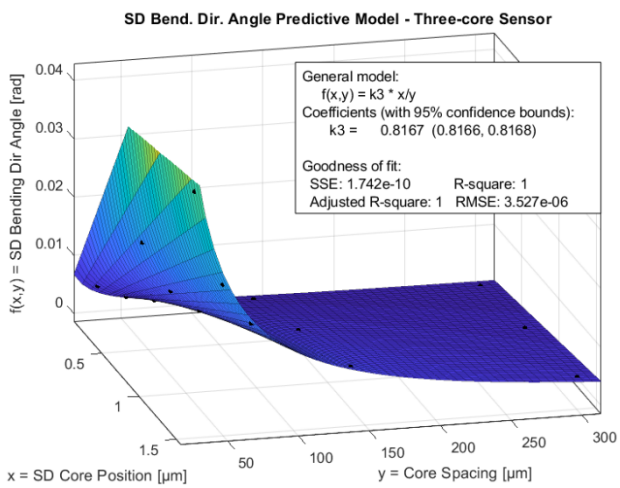

Fig. 7. Bending direction angle SD curve-fitting for a three-core sensor.

In the case of the curvature distribution SD, a four-variable curve was required to fit the data (Eq. 16) with the coefficient k_2. Hence, three distinct curves (see Eq. 18-20), with one coefficient and three variables each, were calibrated at constant values of measured curvature, 0.1, 5.0 and 40.0 m^{-1}. The value of k_2 was then determined by a linear regression analysis considering the coefficients of the three aforementioned curves. Fig. 8 shows, the surface fitting and linear regression of the three-core section geometry.

$$SD\varepsilon^{long} = \boldsymbol{k_1}\,(SDcp \times |\kappa|) \tag{15}$$

$$SD|\kappa| = \boldsymbol{k_2}\,(SDcp \times |\kappa|/r) \tag{16}$$

$$SD\alpha = \boldsymbol{k_3}\,(SDcp/r) \tag{17}$$

$$SD|\kappa|(|\kappa| = 0.1) = \boldsymbol{k'_2}\ (SDcp/r) \quad (18)$$

$$SD|\kappa|(|\kappa| = 5.0) = \boldsymbol{k''_2}\ (SDcp/r) \quad (19)$$

$$SD|\kappa|\ (|\kappa| = 40.0) = \boldsymbol{k'''_2}\ (SDcp/r) \quad (20)$$

where $SDcp$, $SD\varepsilon^{long}$, $SD|\kappa|$ and $SD\alpha$ are respectively the standard deviation of normal frequency distribution of core position errors in μm, longitudinal strain in με, curvature in m^{-1} and bending direction angle in rad, r is the core spacing in μm (distance between the sensor axis and the outer cores), $|\kappa|$ is the measured curvature in m^{-1} and k_1, k_2, k_3, k'_2, k''_2 and k'''_2 are the curves coefficients.

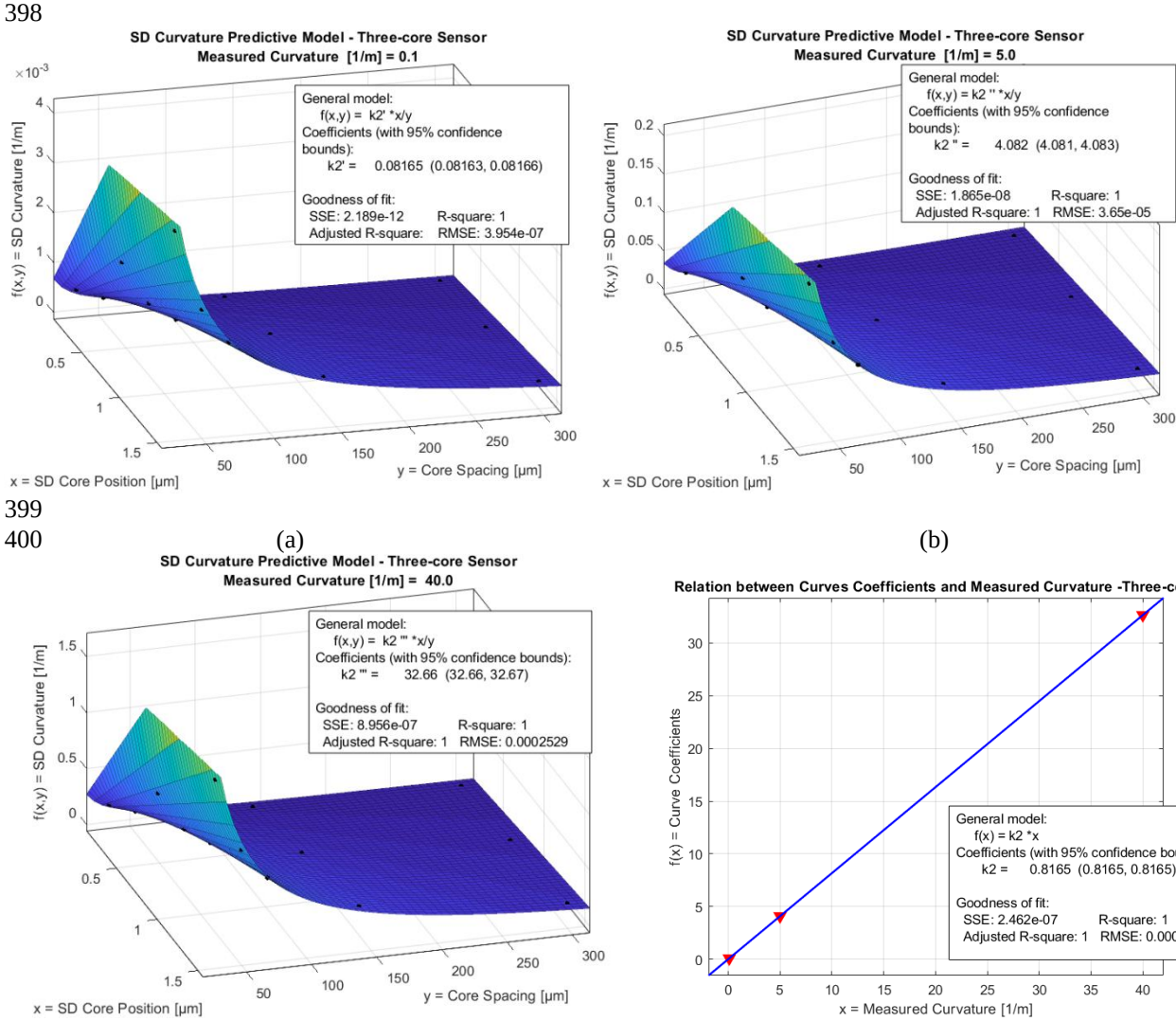

Fig. 8. Curvature SD curve-fitting for a three-core sensor with measured curvature of (a) 0.1 m^{-1}; (b) 5.0 m^{-1}; (c) 40.0 m^{-1}; (d) Relationship between the curve coefficients and measured curvature.

The curves coefficients for the different section geometries and the results of nonlinear regression analysis that measures the goodness of fit are listed in the Table 6:

Table 6. Results of the curve fitting analysis for the three different section geometries in the following order: first 3-core, second 4-core and third 7-core.

Function Equation	f(x,y)	Coefficient	Coef. Value	Coefficient of Determination (R^2)	Root-Mean-Square Error (RMSE)	Sum of Squared Errors (SSE)
$f(x,y) = k_1 x y$	SD ε^{long}	k_1	0.57690	1.000000	0.004288	0.000147
$f(x,y) = k_2' x / y$	SD $\lvert\kappa\rvert$ ($\kappa = 0.1$)	k_2'	0.08165	1.000000	0.000000	0.000000
$f(x,y) = k_2'' x / y$	SD $\lvert\kappa\rvert$ ($\kappa = 5.0$)	k_2''	4.08200	1.000000	0.000037	0.000000
$f(x,y) = k_2''' x / y$	SD $\lvert\kappa\rvert$ ($\kappa = 40.0$)	k_2'''	32.66000	1.000000	0.000253	0.000000
$f(x,y) = k_2 x$	$k_2' k_2'' k_2'''$	k_2	0.81650	1.000000	0.000351	0.000000
$f(x,y) = k_3 x / y$	SD α	k_3	0.81670	1.000000	0.000004	0.000000
$f(x,y) = k_1 x y$	SD ε^{long}	k_1	0.50000	1.000000	0.001380	0.000015
$f(x,y) = k_2' x / y$	SD $\lvert\kappa\rvert$ ($\kappa = 0.1$)	k_2'	0.07071	1.000000	0.000000	0.000000
$f(x,y) = k_2'' x / y$	SD $\lvert\kappa\rvert$ ($\kappa = 5.0$)	k_2''	3.53600	1.000000	0.000021	0.000000
$f(x,y) = k_2''' x / y$	SD $\lvert\kappa\rvert$ ($\kappa = 40.0$)	k_2'''	28.28000	1.000000	0.000207	0.000000
$f(x,y) = k_2 x$	$k_2' k_2'' k_2'''$	k_2	0.70700	1.000000	0.000702	0.000000
$f(x,y) = k_3 x / y$	SD α	k_3	0.70720	1.000000	0.000003	0.000000
$f(x,y) = k_1 x y$	SD ε^{long}	k_1	0.37790	1.000000	0.004876	0.000190
$f(x,y) = k_2' x / y$	SD $\lvert\kappa\rvert$ ($\kappa = 0.1$)	k_2'	0.05774	1.000000	0.000000	0.000000
$f(x,y) = k_2'' x / y$	SD $\lvert\kappa\rvert$ ($\kappa = 5.0$)	k_2''	2.88600	1.000000	0.000026	0.000000
$f(x,y) = k_2''' x / y$	SD $\lvert\kappa\rvert$ ($\kappa = 40.0$)	k_2'''	23.10000	1.000000	0.000142	0.000000
$f(x,y) = k_2 x$	$k_2' k_2'' k_2'''$	k_2	0.57750	1.000000	0.001052	0.000002
$f(x,y) = k_3 x / y$	SD α	k_3	0.57740	1.000000	0.000005	0.000000

It should be noted that Eqs. 16 and 17 can be applied not only to multicore sensors and Optical Fiber Bundle sensors, in which the typical values of core position SD and core spacing are included in the range examined, but also to multiple single-core optical fiber sensors with a higher standard deviation of core position error distribution and core spacing, such as optical inclinometers. In fact, in this last case, the section geometries generally are the same as the one analyzed in this research [11,12]. Besides, the typical values of core position SD and core spacing are a few millimeters or tenths of millimeter and some tens of millimeters, which means that the ratio between these two parameters, which is what enters in the equations, is still inside the range studied (it can easily be verified converting the millimeters into micrometers and substituting the terms into the equations of the predictive models).

Furthermore, since the model coefficients represent the intensity of error propagation (no error propagation when the coefficients are null), there is an interesting improvement in the uncertainty propagation associated with more cores than those in the three-core section, which has the minimum number required for shape sensing. Table 7 shows the percentage reduction in the coefficients of the four-core and seven-core sections compared to the three-core geometry. As mentioned in Section 2, the presence of the central core only affects the accuracy of the longitudinal strain calculation (coefficient k_1), while the seven-core section behaves like a six-core in the other cases.

A good example of application of the predictive models may be the development of optical curvature sensor (optical multicore fiber or optical multi-fiber) for bending of wing aircraft monitoring. As all the engineering applications, it is known the measuring range, taking into consideration what the minimum detectable curvature and the maximum acceptable curvature to avoid damages are, and the required accuracy. Hence, considering the geometrical features of fibers available in the market, it is possible to calculate the uncertainty arising from core position errors, check what of the available fibers fit the requirements and if the errors are acceptable, taking into account that core position errors are not the unique source of errors, which has to be considered [21].

Table 7. Comparison in terms of the percentage reduction of the model coefficients between the three-core section and the four-core and seven-core sections.

Coefficient	Four-core geometry	Seven-core geometry
k_1	13.3299	34.4947
k_2'	13.3987	29.2835
k_2''	13.3758	29.2994
k_2'''	13.4109	29.2713
k_2	13.4109	29.2713
k_3	13.4076	29.3008

Fig. 9 shows the reduced error propagation, in terms of coefficient percentage, with different numbers of cores.

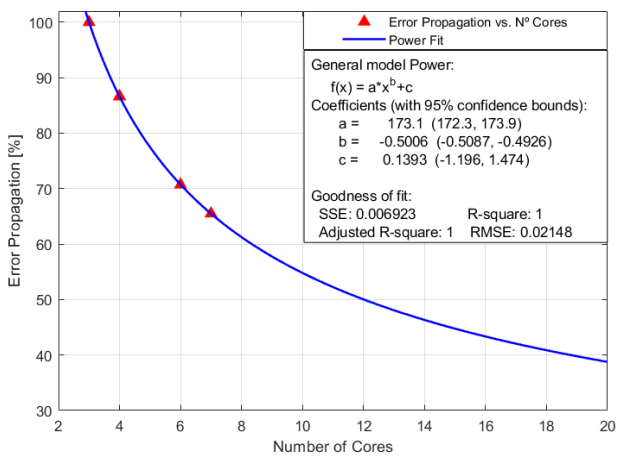

Fig. 9. Variation of propagation errors with number of cores.

6. Conclusions

Innovative shape sensing technology based on strain sensing and used for a number of aerospace, medical, civil, and mechanical engineering applications requires the high-precision calculation of curvature and bending direction.

This research focused on the influence of core position uncertainty, a crucial aspect for shape sensors accuracy, considering both multiple single-core fibers and multicore optical sensors

equipped with distributed or quasi-distributed strain-sensors with three of the most widely employed sensing fiber geometries: the 7-core, 4-core and 3-core. The Monte Carlo technique was proposed to reproduce measurement process with $3 \cdot 10^6$ iterations considering different core spacings and measured curvatures to identify their role in the calculation of longitudinal strain, bending direction and curvature and determine the propagation law of core position uncertainty. A statistical test was performed to verify the significance of the experiment results and a sequence of models were calibrated for each section geometry to define the relationship between the variables considered and make the research outcomes more fruitful and user-friendly. The results obtained were compared with the three section geometries studied.

The above discussion leads to following conclusions:

- Strain plane calculation through Sum of Squared Errors minimization is a valid approach to deal with different shape sensors section geometries, even when there are section asymmetries.
- The MCM is a potent technique for modeling the propagation of core position errors in computing longitudinal strain, bending and direction curvature.
- The core position SD has a linear influence on the frequency distribution of longitudinal strain, bending direction angle and curvature (Section 5.4).
- The SDs of the bending direction angle and curvature distributions strongly depend on core spacing through an inverse relationship, whereas there is no relationship between longitudinal strain SD and core spacing (Section 5.4).
- The measured curvature has no influence on bending direction angle, but linearly influences the curvature and longitudinal strain SD, so that in these cases the sensor accuracy is related not only to aspects of product design, but also to the application (Section 5.4).
- Increasing the number of cores remarkably improves the power-function relationship (Table 7 and Fig. 8).

The study shows the important role of core position errors and underlines the fact that manufacturers do not normally provide information on this aspect. The outcomes successfully identify the propagation laws of core position uncertainty and show the considerable influence of number of cores, core spacing and measured curvature on shape sensor accuracy. The resulting predictive models can support user choices and help manufacturers to identify the parameters that need to be changed to achieve better performance. For example, improving the manufacturing process for higher precision in core positioning, larger core spacing, including more cores, or the performance achievable through different sensor designs.

This study, a continuation of the authors' previous work [21], identifies diverse shape sensor error sources. Future research efforts will involve experimental tests to lay the foundations for the design of new types of shape sensor.

Acknowledgments

This work was carried out within the ITN-FINESSE framework, funded by the European Union's Horizon 2020 Research and Innovation Program under the Marie Sklodowska-Curie Action Grant Agreement N° 722509. It was also supported by the Ministry of Economy and Competitiveness of Spain under the project DIMENSION TEC2017-88029-R.

References

[1] H.F. Pei, J. Teng, J.H. Yin, R. Chen, A review of previous studies on the applications of optical fiber sensors in geotechnical health monitoring, Meas. J. Int. Meas. Confed. 58 (2014) 207–214. doi:10.1016/j.measurement.2014.08.013.

[2] H.Z. Yang, X.G. Qiao, D. Luo, K.S. Lim, W. Chong, S.W. Harun, A review of recent developed and applications of plastic fiber optic displacement sensors, Meas. J. Int. Meas. Confed. 48 (2014) 333–345. doi:10.1016/j.measurement.2013.11.007.

[3] C.K.Y. Leung, K.T. Wan, D. Inaudi, X. Bao, W. Habel, Z. Zhou, J. Ou, M. Ghandehari, H.C. Wu, M. Imai, Review: optical fiber sensors for civil engineering applications, Mater. Struct. 48 (2015) 871–906. doi:10.1617/s11527-013-0201-7.

[4] A. Barrias, J. Casas, S. Villalba, A Review of Distributed Optical Fiber Sensors for Civil Engineering Applications, Sensors. 16 (2016) 748. doi:10.3390/s16050748.

[5] D. Tosi, E. Schena, C. Molardi, S. Korganbayev, Fiber optic sensors for sub-centimeter spatially resolved measurements: Review and biomedical applications, Opt. Fiber Technol. 43 (2018) 6–19. doi:10.1016/j.yofte.2018.03.007.

[6] D. Sartiano, S. Sales, Low Cost Plastic Optical Fiber Pressure Sensor Embedded in Mattress for Vital Signal Monitoring, (2017). doi:10.3390/s17122900.

[7] M.J. Gander, W.N. MacPherson, R. McBride, J.D.C. Jones, L. Zhang, I. Bennion, P.M. Blanchard, J.G. Burnett, a H. Greenaway, Bend mesurement using Bragg gratings in multicore fibre, Electron. Lett. 36 (2000) 2–3.

[8] G.M.H. Flockhart, W.N. MacPherson, J.S. Barton, J.D.C. Jones, L. Zhang, I. Bennion, Two-axis bend measurement with Bragg gratings in multicore optical fiber, Opt. Lett. 28 (2003) 387. doi:10.1364/OL.28.000387.

[9] W.N. MacPherson, G.M.H. Flockhart, R.R.J. Maier, J.S. Barton, J.D.C. Jones, D. Zhao, L. Zhang, I. Bennion, Pitch and roll sensing using fibre Bragg gratings in multicore fibre, Meas. Sci. Technol. 15 (2004) 1642–1646. doi:10.1088/0957-0233/15/8/036.

[10] J.P. Moore, M.D. Rogge, Shape sensing using multi-core fiber optic cable and parametric curve solutions, Opt. Express. 20 (2012) 2967. doi:10.1364/OE.20.002967.

[11] P. Lenke, M. Wendt, K. Krebber, R. Glötzl, Highly sensitive fiber optic inclinometer: easy to transport and easy to install, 21st Int. Conf. Opt. Fibre Sensors. 7753 (2011) 775352-775352–4. doi:10.1117/12.884695.

[12] Y.L. Wang, B. Shi, T.L. Zhang, H.H. Zhu, Q. Jie, Q. Sun, Introduction to an FBG-based inclinometer and its application to landslide monitoring, J. Civ. Struct. Heal. Monit. 5 (2015) 645–653. doi:10.1007/s13349-015-0129-4.

[13] J. Villatoro, A. Van Newkirk, E. Antonio-Lopez, J. Zubia, A. Schülzgen, R. Amezcua-Correa, Ultrasensitive vector bending sensor based on multicore optical fiber., Opt. Lett. 41 (2016) 832–5. doi:10.1364/OL.41.000832.

[14] W.N. MacPherson, M. Silva-Lopez, J.S. Barton, a J. Moore, J.D.C. Jones, D. Zhao, L. Zhang, I. Bennion, N. Metje, D.N. Chapman, C.D.F. Rogers, Tunnel monitoring using multicore fibre displacement sensor, Meas. Sci. Technol. 17 (2006) 1180–1185. doi:10.1088/0957-0233/17/5/S41.

[15] A. Fender, W.N. MacPherson, R.R.J. Maier, J.S. Barton, D.S. George, R.I. Howden, G.W. Smith, B.J.S. Jones, S. McCulloch, X. Chen, R. Suo, L. Zhang, I. Bennion, Two-axis accelerometer based on multicore fibre Bragg gratings, IEEE Sens. J. 8 (2007) 66190Q–66190Q–4. doi:10.1117/12.738411.

[16] P.S. Westbrook, T. Kremp, K.S. Feder, W. Ko, E.M. Monberg, H. Wu, D.A. Simoff, T.F. Taunay, R.M. Ortiz, Continuous Multicore Optical Fiber Grating Arrays for Distributed Sensing Applications, J. Light. Technol. 35 (2017) 1248–1252. doi:10.1109/JLT.2017.2661680.

[17] E.M. Lally, M. Reaves, E. Horrell, S. Klute, M.E. Froggatt, Fiber optic shape sensing for monitoring of flexible structures, in: M. Tomizuka, C.-B. Yun, J.P. Lynch (Eds.), Proc. SPIE - Int. Soc. Opt. Eng., 2012: p. 83452Y. doi:10.1117/12.917490.

[18] X. Yi, F. Niu, J. He, H. Fan, The 3D shape analysis of elastic rod in shape sensing medical robot system, in: 2010 IEEE Int. Conf. Robot. Biomimetics, IEEE, 2010: pp. 1014–1018. doi:10.1109/ROBIO.2010.5723465.

[19] E. Koch, A. Dietzel, Skin attachable flexible sensor array for respiratory monitoring, Sensors Actuators, A Phys. 250 (2016) 138–144. doi:10.1016/j.sna.2016.09.020.

[20] E. Koch, A. Dietzel, Surface reconstruction by means of a flexible sensor array, Sensors Actuators A Phys. 267 (2017) 293–300. doi:10.1016/j.sna.2017.10.023.

[21] I. Floris, S. Sales, P.A. Calderón, J.M. Adam, Measurement uncertainty of multicore optical fiber sensors used to

sense curvature and bending direction, Meas. J. Int. Meas. Confed. 132 (2019) 35–46. doi:10.1016/j.measurement.2018.09.033.

[22] http://itn-finesse.eu/, (n.d.).

[23] L.J. Cooper, A.S. Webb, A. Gillooly, M. Hill, T. Read, P. Maton, J. Hankey, A. Bergonzo, Design and performance of multicore fiber optimized towards communications and sensing applications, in: S. Jiang, M.J.F. Digonnet (Eds.), Proc. SPIE - Int. Soc. Opt. Eng., 2015: p. 93590H. doi:10.1117/12.2076950.

[24] X. Sun, J. Li, D.T. Burgess, M. Hines, B. Zhu, A multicore optical fiber for distributed sensing, 9098 (2014) 1–5. doi:10.1117/12.2050130.

[25] Joint Committee For Guides In Metrology, JCGM 100:2008, Evaluation of measurement data — Guide to the expression of uncertainty in measurement, 2008.

[26] Joint Committee For Guides In Metrology, JCGM 101:2008, Evaluation of measurement data — Supplement 1 to the " Guide to the expression of uncertainty in measurement " — Propagation of distributions using a Monte Carlo method, 2008.

[27] J. Langer, D. a. Singer, Lagrangian Aspects of the Kirchhoff Elastic Rod, SIAM Rev. 38 (1996) 605–618. doi:10.1137/S0036144593253290.

[28] P.S. Westbrook, K.S. Feder, T. Kremp, T.F. Taunay, E. Monberg, J. Kelliher, R. Ortiz, K. Bradley, K.S. Abedin, D. Au, G. Puc, Integrated optical fiber shape sensor modules based on twisted multicore fiber grating arrays, in: I. Gannot (Ed.), 2014: p. 89380H. doi:10.1117/12.2041775.

[29] V. Synek, Effect of insignificant bias and its uncertainty on the coverage probability of uncertainty intervalsPart 2. Evaluation for a found insignificant experimental bias, Talanta. 71 (2007) 1304–1311. doi:10.1016/j.talanta.2006.06.038.

[30] C.E. Papadopoulos, H. Yeung, Uncertainty estimation and Monte Carlo simulation method, Flow Meas. Instrum. 12 (2001) 291–298. doi:10.1016/S0955-5986(01)00015-2.

[31] K. Shahanaghi, P. Nakhjiri, A new optimized uncertainty evaluation applied to the Monte-Carlo simulation in platinum resistance thermometer calibration, Meas. J. Int. Meas. Confed. 43 (2010) 901–911. doi:10.1016/j.measurement.2010.03.008.

[32] A.M. Saviano, F.R. Lourenço, Measurement uncertainty estimation based on multiple regression analysis (MRA) and Monte Carlo (MC) simulations – Application to agar diffusion method, Measurement. 115 (2018) 269–278. doi:10.1016/j.measurement.2017.10.057.

[33] M. Kova evi, D. Nikezi, A. Djordjevich, Monte Carlo simulation of curvature gauges by ray tracing, Meas. Sci. Technol. 15 (2004) 1756–1761. doi:10.1088/0957-0233/15/9/011.

[34] M. Gilman, A brief survey of stopping rules in Monte Carlo simulations, Second Conf. Appl. Simulations. (1968) 16–20.

[35] I.T. Dimov, S. McKee, Monte Carlo Methods for Applied Scientists, (2008) 1–9.

[36] D. Barrera, I. Gasulla, S. Sales, Multipoint Two-Dimensional Curvature Optical Fiber Sensor Based on a Nontwisted Homogeneous Four-Core Fiber, J. Light. Technol. 33 (2015) 2445–2450. doi:10.1109/JLT.2014.2366556.

[37] Z. Zhao, M.A. Soto, M. Tang, L. Thévenaz, Distributed shape sensing using Brillouin scattering in multi-core fibers, Opt. Express. 24 (2016) 25211. doi:10.1364/OE.24.025211.

[38] P.S. Westbrook, T. Kremp, K.S. Feder, W. Ko, E.M. Monberg, H. Wu, D.A. Simoff, S. Shenk, R.M. Ortiz, Performance characteristics of continuously grated multicore sensor fiber, in: Y. Chung, W. Jin, B. Lee, J. Canning, K. Nakamura, L. Yuan (Eds.), 2017: p. 103236I. doi:10.1117/12.2263481.

[39] D. Zheng, J. Madrigal, H. Chen, D. Barrera, S. Sales, Multicore fiber-Bragg-grating-based directional curvature sensor interrogated by a broadband source with a sinusoidal spectrum, Opt. Lett. 42 (2017) 3710–3713. doi:10.1364/OL.42.003710.

[40] U.S. MATLAB R2015a, The MathWorks, Inc., Natick, Massachusetts, MATLAB R2015a, The MathWorks, Inc., Natick, Massachusetts, United States, (n.d.).